

Review

# Graphene on Silicon Photonics: Light Modulation and Detection for Cutting-Edge Communication Technologies

Siqi Yan <sup>1</sup>, Jeremy Adcock <sup>2</sup> and Yunhong Ding <sup>2,\*</sup>

<sup>1</sup> School of Optical and Electrical Information, Huazhong University of Science and Technology, Wuhan 430074, China; siqya@hust.edu.cn

<sup>2</sup> DTU Fotonik, Department of Photonics Engineering, Technical University of Denmark, DK-2800 Lyngby, Denmark; jerad@fotonik.dtu.dk

\* Correspondence: yudin@fotonik.dtu.dk

**Abstract:** Graphene—a two-dimensional allotrope of carbon in a single-layer honeycomb lattice nanostructure—has several distinctive optoelectronic properties that are highly desirable in advanced optical communication systems. Meanwhile, silicon photonics is a promising solution for the next-generation integrated photonics, owing to its low cost, low propagation loss and compatibility with CMOS fabrication processes. Unfortunately, silicon's photodetection responsivity and operation bandwidth are intrinsically limited by its material characteristics. Graphene, with its extraordinary optoelectronic properties has been widely applied in silicon photonics to break this performance bottleneck, with significant progress reported. In this review, we focus on the application of graphene in high-performance silicon photonic devices, including modulators and photodetectors. Moreover, we explore the trend of development and discuss the future challenges of silicon-graphene hybrid photonic devices.

**Keywords:** graphene; silicon photonics; optics communications



**Citation:** Yan, S.; Adcock, J.; Ding, Y. Graphene on Silicon Photonics: Light Modulation and Detection for Cutting-Edge Communication Technologies. *Appl. Sci.* **2022**, *12*, 313. <https://doi.org/10.3390/app12010313>

Academic Editor: Petr Korusenko

Received: 20 November 2021

Accepted: 24 December 2021

Published: 29 December 2021

**Publisher's Note:** MDPI stays neutral with regard to jurisdictional claims in published maps and institutional affiliations.



**Copyright:** © 2021 by the authors. Licensee MDPI, Basel, Switzerland. This article is an open access article distributed under the terms and conditions of the Creative Commons Attribution (CC BY) license (<https://creativecommons.org/licenses/by/4.0/>).

## 1. Introduction

The ongoing fourth industrial revolution [1] is driven by the tremendous quantities of data associated with the internet of things [2], cloud computing [3], and big data analytics [4]. Fast and highly efficient tele- and data-communication systems are essential to support these data intensive technologies. Optical communication technology plays a key role in nearly every aspect of the modern communication links such as access networks, aggregation networks and core networks [5]. Silicon optical interconnect chips, especially silicon modulators and photodetectors, are at the heart of communication networks, thanks to their CMOS compatible fabrication process, cost- and energy-efficient properties [6–8].

To meet the explosive demands of the data traffic, silicon optical interconnect chips need to exhibit extraordinary performance, underscored by the following key merits: bandwidths above 100 GHz, photodetector responsivities larger than 1 A/W, modulation depth larger than 3.5 dB and modulator power consumption less than 30 fJ/bit [9]. Pure silicon devices cannot meet these goals simultaneously owing to the drawbacks of its inherent material properties, such as its indirect bandgap of 1.14 eV and its carrier drift velocity of around 1000 cm<sup>2</sup>/(V·s) [10]. Thanks to the impressive optoelectronic properties of graphene, including its ultra-large heat conductivity [11], ultra-high carrier mobility [12], and ultra-wide light absorption spectrum [13], the hybrid integration of monolayer graphene and silicon photonic devices is a promising solution, with encouraging progress achieved in the last decade [14–16].

In this review, we first analyze the current research status of silicon/graphene hybrid modulators, including thermal-optical modulators and electro-optical modulators. Next, we introduce high-performance silicon/graphene photodetectors, covering both the

photodetection mechanisms and the state-of-the-art performances. Finally, we discuss the challenges and the future trend of the silicon/graphene hybrid devices.

## 2. Physical Properties and Hybrid Graphene/Silicon Fabrication Processes

Graphene, a single-atomic-layer system consisting solely of carbon atoms formed in a hexagonal lattice, holds several distinctive physical properties owing to its unique linear energy dispersion relation [17]. These properties make it an ideal enhancement towards the silicon modulators and detectors. Among these properties, the ultrahigh carrier mobility of graphene is most widely exploited since it enables the ultrafast silicon modulator and photodetector [12,18–20]. Moreover, thanks to the gapless nature of graphene, it absorbs photons in wavelengths ranging from the visible to the infrared. This is highly favorable for photodetection operating in the telecommunications C-band (1530–1565 nm), in which silicon is transparent. Furthermore, graphene's extraordinarily large heat conductivity and relatively low light absorption can be exploited in high-performance nanoscale thermooptic phase shifters within silicon photonics. These properties combine to exhibit superior performance in terms of the tuning efficiency and response time [21–25], when compared to traditional p-i-n or metallic microheater structures, which will be discussed in detail in the Section 3.

The fabrication process of the silicon/graphene hybrid devices typically consists of three steps. The first step is the fabrication of passive silicon photonic circuit. In this step, the grating coupler, waveguides, and other passive elements is fabricated using a lithographic and etching processes. Subsequent planarization then allows the graphene to be placed flat on top of the silicon structures. Generally, graphene is first deposited with a chemical vapor deposition (CVD) process on a copper foil. Then, it is then transferred onto the target area of the chip using a wet or dry transfer process [26]. This step is crucial, and the most challenging, as the quality of the transfer (and therefore of the graphene sample on the device) determines the performance of the graphene-based components on the chip. The third step is the patternization and metallization of the silicon/graphene hybrid chip, which is achieved by standard CMOS fabrication processes. In order to reach ideal Ohmic contact between the graphene and the metal pad, the type of the metal should be carefully chosen since large contact resistance can lead to large RC constant thus low operation speed of the device. Normally, titanium (Ti), palladium (Pd) and platinum (Pt) are ideal choices since they hold low contact resistance with graphene [27].

## 3. High-Performance Modulation Devices Based on Graphene

In optical telecommunications scenarios, optical modulators are used to convert the encoding of electronic data to the optical domain. Any combination of photonic degrees of freedom can be utilized, for example intensity, phase, and/or frequency [28–30]. Afterwards low-loss optical fibers are used to achieve long distance communication links. Integrated silicon optical modulators allow an orders-of-magnitude decrease in size, weight and power in modulation systems, and thus have attracted great attention since their first demonstrations [30].

Among these modulation mechanisms, intensity modulation is most widely applied due to its simplicity. There are two typical methods to realize intensity modulation in integrated silicon chips. One method is to directly alter the absorption of the active medium, and the other is to convert phase modulation to intensity modulation with interference structures, for example using a Mach-Zehnder interferometer (MZI) or a micro-ring resonator (MRR). Both methods rely on the efficient modulation of either the refractive index of the waveguide or the absorption of the active medium. For both types of phase shifter, graphene's impressive optical and electrical properties offer a significant enhancement in key performance metrics, such as bandwidth and power consumption.

### 3.1. Thermo-Optic Modulators Based on Graphene

Thermo-optic phase modulators change the refractive index of the waveguide via a temperature differential. This is typically realized with a metallic microheater fabricated proximally to the silicon waveguide [31–33], or a conducting p-i-n structure close to, or part of the optical waveguide [34]. Typically, a  $\sim 1$   $\mu\text{m}$  layer of silicon dioxide is fabricated between the metallic microheater and waveguide to localize heating to the waveguide, while eliminating the strong absorption light by the metallic microheater (Figure 1a). However, this insulative layer impedes the speed and efficiency of heat transmission from the heater to the waveguide, resulting in high power consumption and low modulation speed. In p-i-n based structures, the induced carriers cause additional optical loss by photonic absorption by mid-band donor states.

Graphene is considered to be an ideal replacement of the metallic microheater as close to transparent, while retaining strong Joule heating properties, removing the requirement an oxide layer (Figure 1a) [35]. Based on this principle, graphene microheaters have been applied in many fields including flexible heaters and heat conductors, while its application as a thermo-optic modulator in silicon photonics was first proposed by Yu et al. in 2014 [21]. Figure 1b shows graphene acting as a heat conductor to deliver heat from a non-local traditional metal heater to the silicon waveguide integrated within a MZI structure. The tuning efficiency is around 0.07 nm/mW while the 90% rising and decaying times (the time it takes for the change in temperature to reach 90% of the maximum value from rest) are 20  $\mu\text{s}$ . It should be noted that in this work graphene only acts as a thermal conductor, rather than a microheater.

In 2015, Bao et al. reported a novel thermo-optic modulator where graphene operates as a transparent microheater fully covering a silicon MRR (Figure 1c). Thanks to the ultrahigh heat conductivity of graphene, the response time of the graphene-based thermo-optic MRR modulator is only 750 ns. Meanwhile, the tuning efficiency is enhanced to 0.1 nm/mW [22]. To further enhance the performance of the thermo-optic silicon modulator based on graphene, the shape of the graphene is patterned to only cover the optical mode, rather than covering the entire device. This method is widely applied in silicon MRRs and micro-disk resonators, with tuning efficiencies of 0.33 nm/mW and 1.67 nm/mW demonstrated respectively, leveraging efficient heat transport from the microheater to the resonator [23,24].

Photonic crystal waveguides are also proposed to enhance graphene microheater efficiency (Figure 1d). In 2017, Yan et al. combined the graphene microheater with a photonic crystal waveguide, enabling a fast-tuning speed of 525 ns and slow-light enhanced tuning efficiency of 1.07 nm/mW [36]. Enhancement via photonic crystal nanocavities has also been demonstrated: Ref. [25] exhibits a tuning efficiency of 3.75 nm/mW, by virtue of the tight confinement of the optical mode within the cavity. These works demonstrate the significant advantages of graphene-based approaches when compared to the conventional microheaters approaches in silicon photonics, in terms of both tuning efficiency and modulation speed.

### 3.2. E-O Modulation

Although the modulation speed of thermo-optic modulator based on graphene microheater can be in the MHz range, this is insufficient for high-speed optical communication systems where the operation bandwidth is in the tens of gigahertz (GHz). Here, electro-optical silicon/graphene modulators, which utilize the electro-optic effect to modulate light, are more applicable. Indeed, graphene's ultra-high carrier mobility may enable modulation speeds of hundred gigahertz, which is particularly attractive for data- and tele-communication systems.

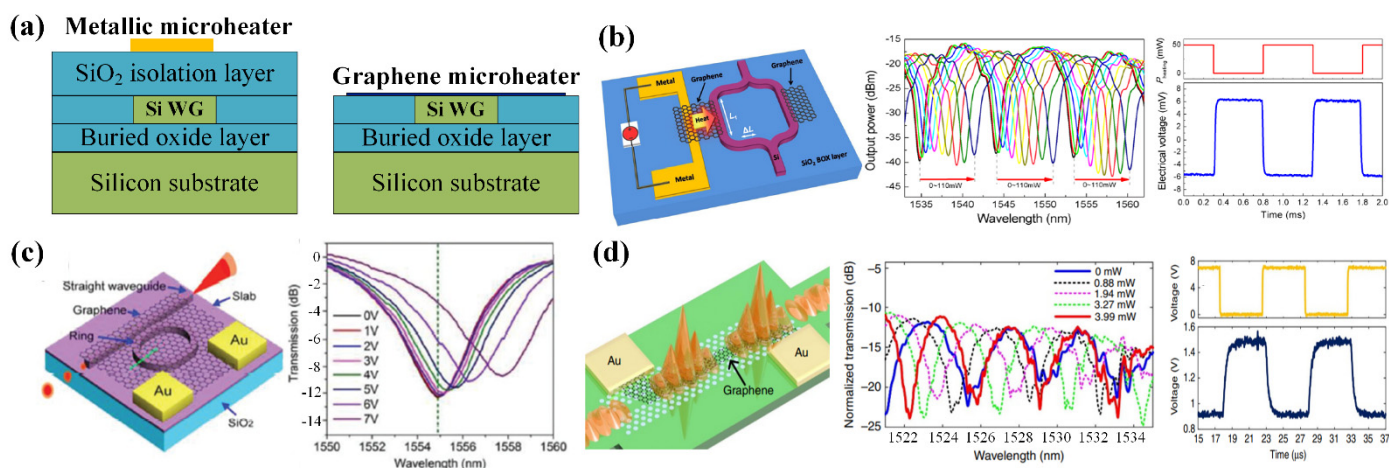


**Figure 1.** Thermo-optic modulators based on graphene for silicon photonics: (a) Schematic of the cross-section of a thermo-optic modulator based on metallic microheater (left) and graphene microheater (right). (b) Silicon thermo-optic modulator employing graphene as the heat conductor [21]. Reprinted from [Appl. Phys. Lett. 105, 251104 (2014)], with the permission of AIP Publishing. (c) MRR silicon thermo-optic modulator covered by graphene microheater. Reproduced from Ref. [22] with permission from the Royal Society of Chemistry [22]. (d) Hybrid integration of silicon photonic crystal structures and the graphene microheater [36].

The first experimental demonstration of a silicon/graphene electro-optical modulator operating at communication wavelengths is reported by Liu et al. in 2011 [37]. Here, a capacitor formed by graphene,  $\text{Al}_2\text{O}_3$ , and silicon waveguide forms the core of the electro-optical modulator. The Fermi level of the graphene sheet is manipulated by applying external voltage on the electrical pad. When the Fermi level is close to the Dirac point, the guided light within the silicon waveguide experiences absorption from graphene, while shifting the Fermi level away from the Dirac point results in transparency. Although this first result is not as impressive as the state-of-the-art silicon modulators, it lays the theoretical foundation for the practical use of graphene within electro-optical modulators.

To enhance the modulation depth of the graphene modulator, various schemes have been reported, focusing on increasing the graphene absorption. The most straightforward method is to use more than one layer of graphene [38–41], which was first proposed by Liu et al. in 2012 [38]. Here, the double layer graphene and a thick oxide layer form a p-i-n junction as the active region for modulation (Figure 2a), leading to a larger modulation depth of 6.5 dB, though the bandwidth is limited to around 1 GHz. By optimizing the RC constant, Giambra et al. showed a double-layer graphene modulator exhibiting a bandwidth of 29 GHz, which is capable of transmitting 50 Gbit/s non-return-to-zero data [40].

Another method to reach higher modulation depths is to employ resonance structures such as photonic crystal cavities and MRRs. Photonic crystal cavities have the advantages of ultra-compact light confinement and could be a promising way to reach higher modulation depth [42–44]. According to Gan et al.'s report, a high modulation more than 10 dB is demonstrated by modulating both the quality factor and the resonance wavelength of the cavity (Figure 2b). Meanwhile, the hybrid integration of a MRR with a graphene monolayer was first introduced in 2014 (Figure 2c) [43]. By altering the resonance wavelength and the quality factor of the MRR, the resonance is modulated with a depth of 40% via gate tuning of the Fermi level in the graphene. Here, the coupling condition of the MRR could also be leveraged to reach higher modulation depths. Ding et al. demonstrated that the modulation depth could be as high as 12.8 dB when the MRR is covered with the optimum length of graphene and working in the slightly under-coupled regime, close to the critical-coupling condition (Figure 2d) [45]. Recently, the silicon slot waveguide is also reported to enhance

the modulation depth of the graphene photodetector, with a modulation depth up to 25 dB experimentally demonstrated [46–49].

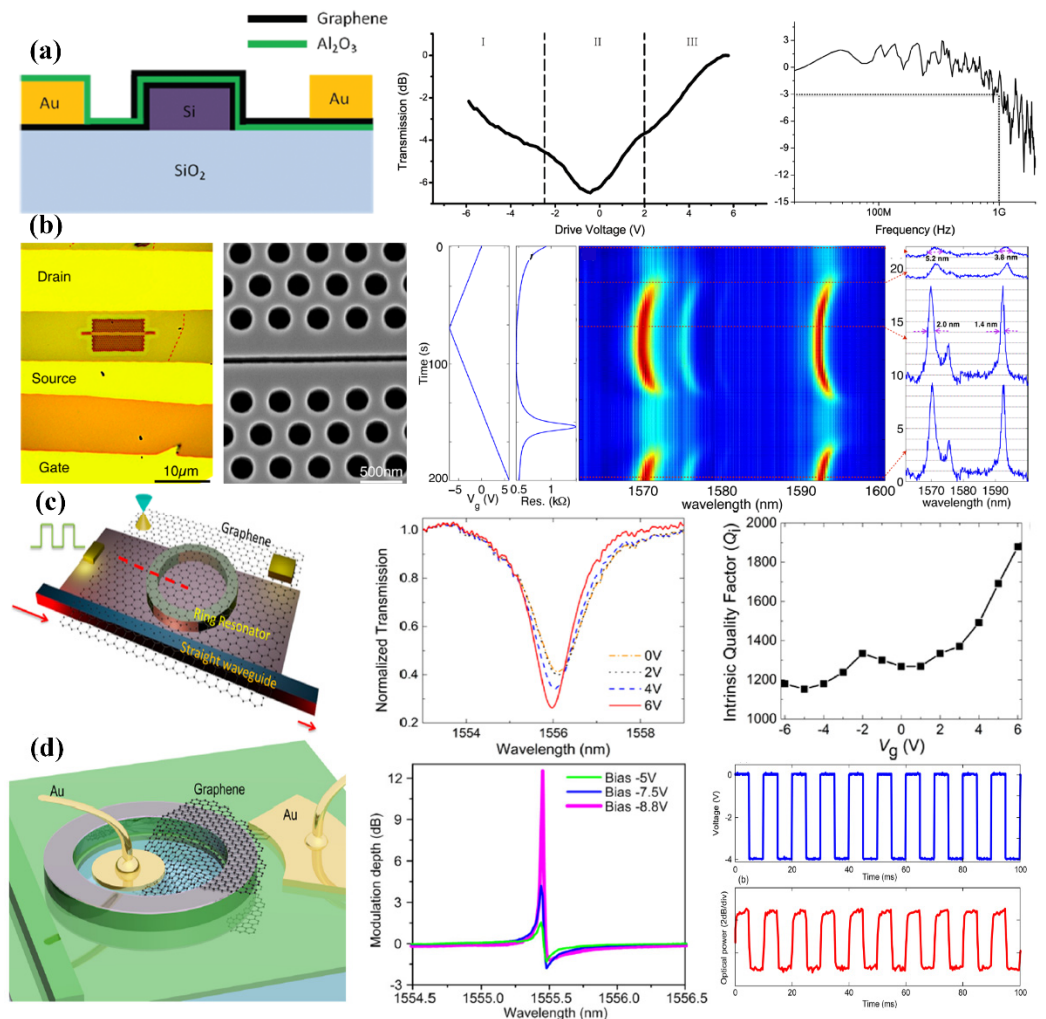


**Figure 2.** Typical graphene/Silicon electro-optical modulators. (a) The schematic and the performance of double-layer graphene modulator. Reprinted with permission from *Nano Lett.* 2012, 12, 3, 1482–1485. Copyright 2012 American Chemical Society. (b) Graphene modulator based on photonic crystal nanocavity. Reprinted with permission from *Nano Lett.* 2013, 13, 2, 691–696. Copyright 2013 American Chemical Society. (c) Graphene modulator based on MRR. Reprinted with permission from *Nano Lett.* 2014, 14, 12, 6811–6815. Copyright 2014 American Chemical Society. (d) High modulation depth graphene modulator based on altering the coupling condition of MRR. Reprinted with permission from *Nano Lett.* 2015, 15, 7, 4393–4400. Copyright 2015 American Chemical Society.

Although the modulation depths in the above-mentioned devices were optimized to an impressive scale, the modulation bandwidth was limited to less than 1 GHz. This is mostly due to the large RC constant of the circuit. To address this issue, the Lipson group proposed a graphene modulator with a graphene monolayer replacing the metal pad within the classical capacitor structure of the modulator, allowing the ultra-high carrier mobility of graphene to be fully utilized. This resulted in a high modulation bandwidth of 30 GHz and a strong modulation depth of 15 dB [19]. Moreover, they also reported a high-performance graphene modulator at cryogenic temperature with an intrinsic bandwidth of 200 GHz [50]. Most recently, a high-performance modulator utilizing a 2D–3D dielectric integration in a high-quality encapsulated graphene device was used to exhibit a ~39 GHz bandwidth, resulting in a three-fold increase in modulation efficiency when compared

to previously reported high-speed modulators [20]. Meanwhile, the electro absorption graphene modulator could also be an ideal candidate as a photonic neuron thresholder, as reported by Volker's group in 2021 [51]. Besides the intensity modulator, the phase modulator based on graphene with a modulation efficiency of  $0.28 \text{ V}\cdot\text{cm}$  and an operation bandwidth of 5 GHz has also been demonstrated [52].

#### 4. High-Performance Photodetector Based on Graphene

Due to its transparency in the telecommunications C-band near 1550 nm, silicon is inefficient in converting light into an electrical signal. Up to now, the mainstream of integrated photodetectors in silicon photonics for the communication wavelengths includes employing germanium (Ge) or monolayer graphene as photodetection material [53,54]. Ge-Si hybrid photodetectors have been widely studied and reached significant maturity thanks to their ability to absorb light in the telecommunications band near 1550 nm. High responsivity larger than  $1 \text{ A/W}$  has been achieved and an impressive bandwidth of 265 GHz has been demonstrated recently [53,55]. Compared to Ge/Si photodetectors, graphene/Si photodetectors hold great potential in reaching ultra large operation bandwidth thanks to the ultrahigh carrier mobility of graphene as well as its absorption ability in a broader wavelength range. For graphene/silicon photodetectors, there are three different mechanisms for the photodetection, which are photovoltaic effect (PV), photo-thermoelectric effect (PTE) and photo-bolometric effect (PB). The graphene photodetectors based on these three mechanisms are discussed in detail below.

The PV effect relies on the separation of photoexcited electrons and holes by an applied electric field to generate photocurrent, which can be utilized by graphene/silicon photodetector structures with normal light incidence [53,54]. As the representative work of early endeavors in graphene-based photodetectors, Xia et al. demonstrated that the graphene/Si photodetectors can reach 40 GHz [55]. Moreover, the intrinsic response time of graphene photodetectors is experimentally demonstrated to be 2.1 ps, indicating a high bandwidth of 262 GHz (Figure 3a) [56].

However, the responsivities of graphene-based photodetectors with normal light incidence are normally low. To increase the light-graphene interaction and obtain better performances, waveguide-based photodetectors have been extensively researched [18,46,57–59]. A typical waveguide integrated structure is shown in Figure 3b [46]. In their design, the graphene lies on top of the silicon slot waveguide as the absorption layer. Here, the graphene monolayer absorbs the light within the waveguide mode's evanescent field, and a responsivity of  $0.273 \text{ A/W}$  is measured.

Meanwhile, hybrid integration of the silicon waveguide and graphene could also be fabricated at the wafer-scale, thanks to its low fabrication complexity [60]. The proposed photodetector holds a bandwidth of 41 GHz and the maximum responsivity is  $46 \text{ mA/W}$ . To further optimize the performance of the photodetector, Ding et al. proposed a waveguide-coupled integrated graphene plasmonic photodetector (Figure 3c) [57]. The plasmonic slot waveguide is formed by two different metallic slabs with a gap of 120 nm. This structure induces subwavelength light confinement within the surface of the graphene, dramatically increasing light absorption within the graphene. Meanwhile, different types of metal cause different doping levels in the graphene, enhancing the internal electrical field in the gap and more effectively separating the photogenerated carriers, leading to a high responsivity. Owing to these two points, the device features responsivity up to  $0.36 \text{ A/W}$  and an operation bandwidth larger than 110 GHz.

When the plasmonic gap becomes even narrower (less than 50 nm), there exist a competition between the PV and PB effect within the photodetection process, as Ma et al. thoroughly investigated [61]. An impressively high responsivity of  $0.7 \text{ A/W}$  at 1310 nm is achieved based on their work with PB effect. The PB effect refers to the modification of the channel resistance by either a change in the number of carriers or a change of the temperature-dependent carrier mobility. Thus, the PB effect leads to a negative photocurrent due to the increased channel resistance caused by the smaller mean free path

induced by a temperature change due to photon absorption. A typical work based on PB effect is reported by Ma Ping employing a bowtie structure to reach a high responsivity of 0.5 A/W and a bandwidth of 110 GHz (Figure 4a) [62]. Wang et al. demonstrated a coherent, plasmonic-structure-based graphene optical receiver (Figure 4b) which is capable of the reception of both a 200 Gbit/s quadrature phase-shift keying (QPSK) signal and a 240 Gbit/s 16 quadrature amplitude modulation (16 QAM) signal on a single-polarization carrier, thanks to the ultrahigh operation bandwidth of the graphene photodetector [58]. Finally, a plasmonic/silicon hybrid graphene photodetector covering 1.55  $\mu\text{m}$  and 2  $\mu\text{m}$  is reported by Guo et al. where the responsivity is 0.07 A/W and 0.4 A/W at 1.55  $\mu\text{m}$  and 2  $\mu\text{m}$  respectively [63].

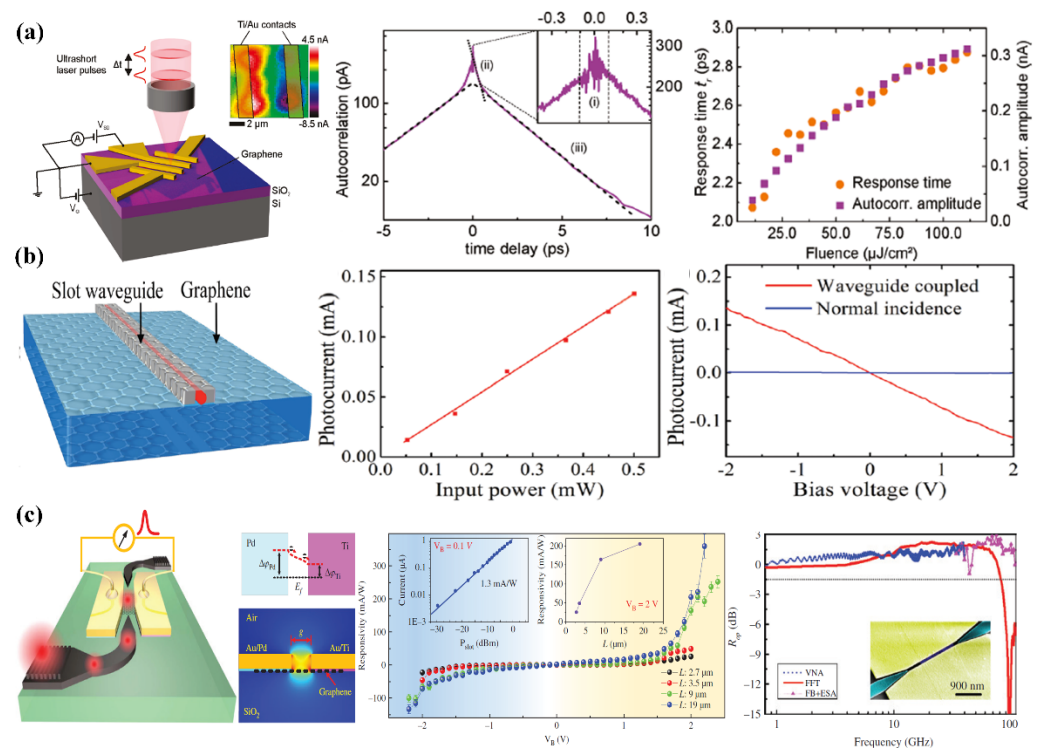


**Figure 3.** Graphene/silicon photodetector based on PV effect. (a) First graphene photodetector operating at 1550 nm. Reprinted with permission from *Nano Lett.* 2011, 11, 7, 2804–2808. Copyright 2011 American Chemical Society. (b) The graphene photodetector based on the silicon slot waveguide. Reproduced from Ref. [49] with permission from the Royal Society of Chemistry [56]. (c) The plasmonic enhanced high-performance graphene photodetector [57].

From the above-mentioned works on plasmonic graphene photodetectors, we can conclude that plasmonic structures can dramatically optimize both the responsivity and the bandwidth of graphene-based receivers. Metallic absorption remains an obstacle, acting to reduce responsivity, since its characteristic absorption does not contribute to the photocurrent. To address this issue, Yan et al. proposed and demonstrated a double slot structure consisting of both the silicon slot waveguide and the plasmonic slot waveguide (Figure 4c) [59]. By optimizing the structural parameters, the metallic absorption is reduced to 0.2 dB/ $\mu\text{m}$  and the responsivity increased to 0.6 A/W.

Besides the PV and PB effect, the PTE effect has also recently been employed in silicon/graphene photodetectors. The PTE effect uses on the photon-induced electron temperature difference between two different graphene doping regions, which is normally achieved by external gating. Thus, the photocurrent is generated by an optically induced temperature gradient, which is proportional to the Seebeck coefficient. By optimizing the gate and source voltages simultaneously, a maximum responsivity of 0.36 A/W and a 3-dB operation bandwidth of 42 GHz is reached [64].

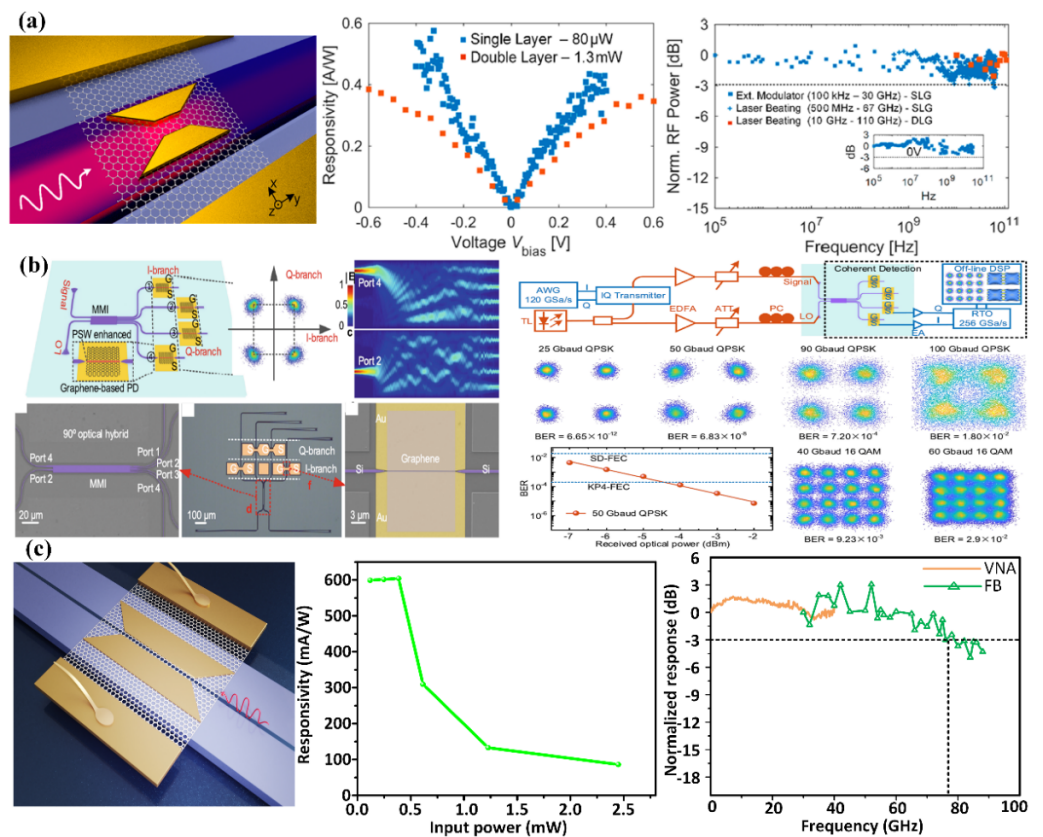


**Figure 4.** Graphene/silicon photodetectors based on PB effect. (a) Plasmonic enhanced graphene photodetector based on bowtie structure. Reprinted with permission from *ACS Photonics* 2019, 6, 1, 154–161. Copyright 2019 American Chemical Society. (b) Coherent optical receiver based on four graphene photodetectors [58]. (c) Double-slot graphene photodetector with a high responsivity [59].

Moreover, photodetectors based on PTE effect can directly convert the optical signal to voltage signal, removing the need for a transimpedance amplifier. Various structures including photonic crystal waveguides [65], micro-ring resonators [66] and double layer graphene [67] have been employed to enhance the light-matter interaction of the PTE effect, reaching impressive performances, such as responsivity higher than 90 V/W and operation bandwidths larger than 65 GHz. Although the external gating function adds complexity to the fabrication process compared to the photodetectors based on PV and PB effect, the PTE graphene photodetector is appealing to industry since it supports the direct connection between the photodetector and the read-out electric circuit. The performances of a typical graphene/silicon photodetector and state-of-the-art photodetectors based on conventional bulk materials is compared in Table 1. Graphene/silicon photodetector can achieve high ultra-high bandwidth more than 110 GHz, thanks to the ultrahigh carrier mobility of graphene. The responsivity of graphene photodetector is comparable with the other material platforms and can be further improved with further optimization by enhancing the light-graphene overlap and interaction.

**Table 1.** Comparison of the key parameters of the state-of-the-art photodetectors based on different materials.

Absorption Material	Responsivity	Bandwidth	Size	Operation Wavelength Range
InGaAs [68]	0.68 A/W	32 GHz	1 $\mu$ m	1260 nm~1360 nm
InP [69]	0.8 A/W	40 GHz	5 $\mu$ m	1240 nm~1650 nm
InP [70]	0.5 A/W	130 GHz	N. A.	1310 nm and 1550 nm

Table 1. Cont.

Absorption Material	Responsivity	Bandwidth	Size	Operation Wavelength Range
$\alpha$ -Ge [71]	0.35 A/W	>100 GHz	20 $\mu$ m	1270 nm~1330 nm
Ge [55]	0.3 A/W	265 GHz	10 $\mu$ m	1550 nm
Graphene [57]	0.36 A/W	>110 GHz	20 $\mu$ m	1540 nm
Graphene [59]	0.6 A/W	78 GHz	30 $\mu$ m	1550 nm
Graphene [62]	0.5 A/W	>110 GHz	6 $\mu$ m	1480 nm~1620 nm
Graphene [63]	0.4 A/W	>40 GHz	20 $\mu$ m	1550 nm and 2000 nm

## 5. Outlook

In the past decade, we have witnessed the impressive rise of graphene within silicon photonics. Silicon photonic modulators and photodetectors with outstanding performances have been reported by several groups, leveraging to the exceptional properties of graphene. However, there are several challenges that hinder further development of silicon/graphene hybrid devices.

The first is to include graphene structures in optimized foundry processes for commercial, wafer-scale fabrication featuring silicon/graphene components. Up to now, most reports rely on the wet transfer of CVD-grown or exfoliated graphene onto the target substrate. This is suitable for prototype demonstrations, but the typical uniformity of the fabricated devices is lacking. Moreover, the wet transfer process can induce particles that significantly increase the transmission loss of the silicon chip. Fortunately, there is already exciting progress on this front [72,73], and we expect wafer-scale silicon/graphene hybrid devices without the issue of uniformity and excess loss soon.

The second is enhancing the light-graphene interaction. Although the atomic thickness of graphene has brought advantages in certain applications—especially the transparent microheater—it also causes low modulation depth and low responsivity in the photodetector. A lot of effort has been dedicated to enhancing the absorption of the graphene layer and significant progress has been made. However, the overall performance in terms of the modulation depth and responsivity so far only matches devices based on bulk materials and is achieved at the expense of sacrificing bandwidth. Therefore, further enhancing the light-graphene interaction while maintaining the advantages of the graphene-based devices remains a challenging but extremely valuable topic.

Overall, both silicon photonics and graphene technology are still in rapid development, while the hybrid integration of these two cutting-edge platforms holds great potential. We believe that once the above-mentioned challenges are fully addressed, hybrid silicon/graphene optoelectronic devices will enable truly new technological capability, both in industry and for the scientific community.

**Author Contributions:** Conceptualization, S.Y. and Y.D.; methodology, S.Y. and Y.D.; writing—original draft preparation, S.Y.; writing—review and editing, S.Y., J.A. and Y.D. All authors have read and agreed to the published version of the manuscript.

**Funding:** This work was funded by QUANPIC project sponsored by VILLUM FONDEN (No. 00025298).

**Institutional Review Board Statement:** Not applicable.

**Informed Consent Statement:** Not applicable.

**Conflicts of Interest:** The authors declare no conflict of interest.

## References

- Xu, M.; David, J.M.; Kim, S.H. The fourth industrial revolution: Opportunities and challenges. *Int. J. Financ. Res.* **2018**, *9*, 90–95. [[CrossRef](#)]
- Ashton, K. That ‘Internet of Things’ thing. *RFID J.* **2009**, *22*, 97–114.
- Wang, L.; Von Laszewski, G.; Younge, A.; He, X.; Kunze, M.; Tao, J.; Fu, C. Cloud computing: A perspective study. *New Gener. Comput.* **2010**, *28*, 137–146. [[CrossRef](#)]

4. Tsai, C.-W.; Lai, C.-F.; Chao, H.-C.; Vasilakos, A.V. Big data analytics: A survey. *J. Big Data* **2015**, *2*, 21. [[CrossRef](#)]
5. Miller, S. *Optical Fiber Telecommunications*; Elsevier: Amsterdam, The Netherlands, 2012.
6. Jalali, B.; Fathpour, S. Silicon photonics. *J. Lightwave Technol.* **2006**, *24*, 4600–4615. [[CrossRef](#)]
7. Soref, R. The past, present, and future of silicon photonics. *IEEE J. Sel. Top. Quantum Electron.* **2006**, *12*, 1678–1687. [[CrossRef](#)]
8. Thomson, D.; Zilkie, A.; Bowers, J.E.; Komljenovic, T.; Reed, G.T.; Vivien, L.; Marris-Morini, D.; Cassan, E.; Virost, L.; Fédéli, J.-M. Roadmap on silicon photonics. *J. Opt.* **2016**, *18*, 073003. [[CrossRef](#)]
9. Miller, D.A. Device requirements for optical interconnects to silicon chips. *Proc. IEEE* **2009**, *97*, 1166–1185. [[CrossRef](#)]
10. Canali, C.; Majni, G.; Minder, R.; Ottaviani, G. Electron and hole drift velocity measurements in silicon and their empirical relation to electric field and temperature. *IEEE Trans. Electron. Devices* **1975**, *22*, 1045–1047. [[CrossRef](#)]
11. Balandin, A.A.; Ghosh, S.; Bao, W.; Calizo, I.; Teweldebrhan, D.; Miao, F.; Lau, C.N. Superior Thermal Conductivity of Single-Layer Graphene. *Nano Lett.* **2008**, *8*, 902–907. [[CrossRef](#)] [[PubMed](#)]
12. Ponomarenko, L.A.; Yang, R.; Mohiuddin, T.M.; Katsnelson, M.I.; Novoselov, K.S.; Morozov, S.V.; Zhukov, A.A.; Schedin, F.; Hill, E.W.; Geim, A.K. Effect of a high- $\kappa$  environment on charge carrier mobility in graphene. *Phys. Rev. Lett.* **2009**, *102*, 206603. [[CrossRef](#)] [[PubMed](#)]
13. Falkovsky, L.A. Optical properties of graphene. *J. Phys. Conf. Ser.* **2008**, *129*, 012004. [[CrossRef](#)]
14. Kim, K.; Choi, J.-Y.; Kim, T.; Cho, S.-H.; Chung, H.-J. A role for graphene in silicon-based semiconductor devices. *Nature* **2011**, *479*, 338–344. [[CrossRef](#)] [[PubMed](#)]
15. Youngblood, N.; Li, M. Integration of 2D materials on a silicon photonics platform for optoelectronics applications. *Nanophotonics* **2017**, *6*, 1205–1218. [[CrossRef](#)]
16. Akinwande, D.; Huyghebaert, C.; Wang, C.-H.; Serna, M.I.; Goossens, S.; Li, L.-J.; Wong, H.S.P.; Koppens, F.H.L. Graphene and two-dimensional materials for silicon technology. *Nature* **2019**, *573*, 507–518. [[CrossRef](#)]
17. Novoselov, K.S.; Geim, A.K.; Morozov, S.V.; Jiang, D.; Katsnelson, M.I.; Grigorieva, I.V.; Dubonos, S.V.; Firsov, A.A. Two-dimensional gas of massless Dirac fermions in graphene. *Nature* **2005**, *438*, 197–200. [[CrossRef](#)] [[PubMed](#)]
18. Gan, X.; Shiue, R.-J.; Gao, Y.; Meric, I.; Heinz, T.F.; Shepard, K.; Hone, J.; Assefa, S.; Englund, D. Chip-integrated ultrafast graphene photodetector with high responsivity. *Nat. Photonics* **2013**, *7*, 883–887. [[CrossRef](#)]
19. Phare, C.T.; Daniel Lee, Y.-H.; Cardenas, J.; Lipson, M. Graphene electro-optic modulator with 30 GHz bandwidth. *Nat. Photonics* **2015**, *9*, 511–514. [[CrossRef](#)]
20. Agarwal, H.; Terrés, B.; Orsini, L.; Montanaro, A.; Soriano, V.; Pantouvaki, M.; Watanabe, K.; Taniguchi, T.; van Thourhout, D.; Romagnoli, M.; et al. 2D-3D integration of hexagonal boron nitride and a high- $\kappa$  dielectric for ultrafast graphene-based electro-absorption modulators. *Nat. Commun.* **2021**, *12*, 1070. [[CrossRef](#)]
21. Yu, L.; Dai, D.; He, S. Graphene-based transparent flexible heat conductor for thermally tuning nanophotonic integrated devices. *Appl. Phys. Lett.* **2014**, *105*, 251104. [[CrossRef](#)]
22. Gan, S.; Cheng, C.; Zhan, Y.; Huang, B.; Gan, X.; Li, S.; Lin, S.; Li, X.; Zhao, J.; Chen, H.; et al. A highly efficient thermo-optic microring modulator assisted by graphene. *Nanoscale* **2015**, *7*, 20249–20255. [[CrossRef](#)]
23. Schall, D.; Mohsin, M.; Sagade, A.A.; Otto, M.; Chmielak, B.; Suckow, S.; Giesecke, A.L.; Neumaier, D.; Kurz, H. Infrared transparent graphene heater for silicon photonic integrated circuits. *Opt. Express* **2016**, *24*, 7871–7878. [[CrossRef](#)]
24. Yu, L.; Yin, Y.; Shi, Y.; Dai, D.; He, S. Thermally tunable silicon photonic microdisk resonator with transparent graphene nanoheaters. *Optica* **2016**, *3*, 159–166. [[CrossRef](#)]
25. Xu, Z.; Qiu, C.; Yang, Y.; Zhu, Q.; Jiang, X.; Zhang, Y.; Gao, W.; Su, Y. Ultra-compact tunable silicon nanobeam cavity with an energy-efficient graphene micro-heater. *Opt. Express* **2017**, *25*, 19479–19486. [[CrossRef](#)]
26. Suk, J.W.; Kitt, A.; Magnuson, C.W.; Hao, Y.; Ahmed, S.; An, J.; Swan, A.K.; Goldberg, B.B.; Ruoff, R.S. Transfer of CVD-Grown Monolayer Graphene onto Arbitrary Substrates. *ACS Nano* **2011**, *5*, 6916–6924. [[CrossRef](#)]
27. Matsuda, Y.; Deng, W.-Q.; Goddard, W.A. Contact Resistance for “End-Contacted” Metal–Graphene and Metal–Nanotube Interfaces from Quantum Mechanics. *J. Phys. Chem. C* **2010**, *114*, 17845–17850. [[CrossRef](#)]
28. Reed, G.T.; Mashanovich, G.; Gardes, F.Y.; Thomson, D.J. Silicon optical modulators. *Nat. Photonics* **2010**, *4*, 518–526. [[CrossRef](#)]
29. Almeida, V.R.; Barrios, C.A.; Panepucci, R.R.; Lipson, M. All-optical control of light on a silicon chip. *Nature* **2004**, *431*, 1081–1084. [[CrossRef](#)]
30. Xu, Q.; Schmidt, B.; Pradhan, S.; Lipson, M. Micrometre-scale silicon electro-optic modulator. *Nature* **2005**, *435*, 325–327. [[CrossRef](#)]
31. Fegadolli, W.S.; Vargas, G.; Wang, X.; Valini, F.; Barea, L.A.M.; Oliveira, J.E.B.; Frateschi, N.; Scherer, A.; Almeida, V.R.; Panepucci, R.R. Reconfigurable silicon thermo-optical ring resonator switch based on Vernier effect control. *Opt. Express* **2012**, *20*, 14722–14733. [[CrossRef](#)] [[PubMed](#)]
32. Atabaki, A.H.; Hosseini, E.S.; Eftekhari, A.A.; Yegnanarayanan, S.; Adibi, A. Optimization of metallic microheaters for high-speed reconfigurable silicon photonics. *Opt. Express* **2010**, *18*, 18312–18323. [[CrossRef](#)]
33. Dong, P.; Qian, W.; Liang, H.; Shafiiha, R.; Feng, D.; Li, G.; Cunningham, J.E.; Krishnamoorthy, A.V.; Asghari, M. Thermally tunable silicon racetrack resonators with ultralow tuning power. *Opt. Express* **2010**, *18*, 20298–20304. [[CrossRef](#)]
34. Harris, N.C.; Ma, Y.; Mower, J.; Baehr-Jones, T.; Englund, D.; Hochberg, M.; Galland, C. Efficient, compact and low loss thermo-optic phase shifter in silicon. *Opt. Express* **2014**, *22*, 10487–10493. [[CrossRef](#)]
35. Khan, U.; Kim, T.-H.; Lee, K.H.; Lee, J.-H.; Yoon, H.-J.; Bhatia, R.; Sameera, I.; Seung, W.; Ryu, H.; Falconi, C.; et al. Self-powered transparent flexible graphene microheaters. *Nano Energy* **2015**, *17*, 356–365. [[CrossRef](#)]

36. Yan, S.; Zhu, X.; Frandsen, L.H.; Xiao, S.; Mortensen, N.A.; Dong, J.; Ding, Y. Slow-light-enhanced energy efficiency for graphene microheaters on silicon photonic crystal waveguides. *Nat. Commun.* **2017**, *8*, 14411. [[CrossRef](#)] [[PubMed](#)]
37. Liu, M.; Yin, X.; Ulin-Avila, E.; Geng, B.; Zentgraf, T.; Ju, L.; Wang, F.; Zhang, X. A graphene-based broadband optical modulator. *Nature* **2011**, *474*, 64–67. [[CrossRef](#)]
38. Liu, M.; Yin, X.; Zhang, X. Double-Layer Graphene Optical Modulator. *Nano Lett.* **2012**, *12*, 1482–1485. [[CrossRef](#)]
39. Koester, S.J.; Li, M. High-speed waveguide-coupled graphene-on-graphene optical modulators. *Appl. Phys. Lett.* **2012**, *100*, 171107. [[CrossRef](#)]
40. Giambra, M.A.; Soriano, V.; Miseikis, V.; Marconi, S.; Montanaro, A.; Galli, P.; Pezzini, S.; Coletti, C.; Romagnoli, M. High-speed double layer graphene electro-absorption modulator on SOI waveguide. *Opt. Express* **2019**, *27*, 20145–20155. [[CrossRef](#)] [[PubMed](#)]
41. Cheng, Z.; Zhu, X.; Galili, M.; Frandsen, L.H.; Hu, H.; Xiao, S.; Dong, J.; Ding, Y.; Oxenløwe, L.K.; Zhang, X. Double-layer graphene on photonic crystal waveguide electro-absorption modulator with 12 GHz bandwidth. *Nanophotonics* **2020**, *9*, 2377–2385. [[CrossRef](#)]
42. Gan, X.; Shiue, R.-J.; Gao, Y.; Mak, K.F.; Yao, X.; Li, L.; Szep, A.; Walker, D.; Hone, J.; Heinz, T.F.; et al. High-Contrast Electrooptic Modulation of a Photonic Crystal Nanocavity by Electrical Gating of Graphene. *Nano Lett.* **2013**, *13*, 691–696. [[CrossRef](#)]
43. Qiu, C.; Gao, W.; Vajtai, R.; Ajayan, P.M.; Kono, J.; Xu, Q. Efficient Modulation of 1.55  $\mu\text{m}$  Radiation with Gated Graphene on a Silicon Microring Resonator. *Nano Lett.* **2014**, *14*, 6811–6815. [[CrossRef](#)]
44. Mao, D.; Cheng, C.; Wang, F.; Xiao, Y.; Li, T.; Chang, L.; Soman, A.; Kananen, T.; Zhang, X.; Krainak, M.; et al. Device Architectures for Low Voltage and Ultrafast Graphene Integrated Phase Modulators. *IEEE J. Sel. Top. Quantum Electron.* **2021**, *27*, 21. [[CrossRef](#)]
45. Ding, Y.; Zhu, X.; Xiao, S.; Hu, H.; Frandsen, L.H.; Mortensen, N.A.; Yvind, K. Effective Electro-Optical Modulation with High Extinction Ratio by a Graphene–Silicon Microring Resonator. *Nano Lett.* **2015**, *15*, 4393–4400. [[CrossRef](#)]
46. Shu, H.; Su, Z.; Huang, L.; Wu, Z.; Wang, X.; Zhang, Z.; Zhou, Z. Significantly High Modulation Efficiency of Compact Graphene Modulator Based on Silicon Waveguide. *Sci. Rep.* **2018**, *8*, 991. [[CrossRef](#)]
47. Zhu, Y.; Deng, C.; Huang, L.; Hu, G.; Yun, B.; Zhang, R.; Cui, Y. Hybrid plasmonic graphene modulator with buried silicon waveguide. *Opt. Commun.* **2020**, *456*, 124559. [[CrossRef](#)]
48. Kovacevic, G.; Phare, C.; Set, S.Y.; Lipson, M.; Yamashita, S. Ultra-high-speed graphene optical modulator design based on tight field confinement in a slot waveguide. *Appl. Phys. Express* **2018**, *11*, 065102. [[CrossRef](#)]
49. Luan, C.; Liu, Y.; Ding, Y.; Hu, H. 2- $\mu\text{m}$  high-speed graphene electro-optic modulator based on silicon slot microring resonator. In Proceedings of the Conference on Lasers and Electro-Optics, Washington, DC, USA, 10–15 May 2020; p. JTh2F.34.
50. Lee, B.S.; Kim, B.; Freitas, A.P.; Mohanty, A.; Zhu, Y.; Bhatt, G.R.; Hone, J.; Lipson, M. High-performance integrated graphene electro-optic modulator at cryogenic temperature. *Nanophotonics* **2021**, *10*, 99–104. [[CrossRef](#)]
51. Amin, R.; George, J.K.; Wang, H.; Maiti, R.; Ma, Z.; Dalir, H.; Khurgin, J.B.; Sorger Volker, J. An ITO–graphene heterojunction integrated absorption modulator on Si-photonics for neuromorphic nonlinear activation. *APL Photonics* **2021**, *6*, 120801. [[CrossRef](#)]
52. Soriano, V.; Midrio, M.; Contestabile, G.; Asselberghs, I.; Van Campenhout, J.; Huyghebaert, C.; Goykhman, I.; Ott, A.K.; Ferrari, A.C.; Romagnoli, M. Graphene–silicon phase modulators with gigahertz bandwidth. *Nat. Photonics* **2018**, *12*, 40–44. [[CrossRef](#)]
53. Benedikovic, D.; Virost, L.; Aubin, G.; Amar, F.; Szelag, B.; Karakus, B.; Hartmann, J.-M.; Alonso-Ramos, C.; Roux, X.L.; Crozat, P.; et al. 25 Gbps low-voltage hetero-structured silicon-germanium waveguide pin photodetectors for monolithic on-chip nanophotonic architectures. *Photonics Res.* **2019**, *7*, 437–444. [[CrossRef](#)]
54. Benedikovic, D.; Virost, L.; Aubin, G.; Hartmann, J.-M.; Amar, F.; Le Roux, X.; Alonso-Ramos, C.; Cassan, E.; Marris-Morini, D.; Crozat, P.; et al. 40 Gbps heterostructure germanium avalanche photo receiver on a silicon chip. *Optica* **2020**, *7*, 775–783. [[CrossRef](#)]
55. Lischke, S.; Peczek, A.; Morgan, J.S.; Sun, K.; Steckler, D.; Yamamoto, Y.; Korndörfer, F.; Mai, C.; Marschmeyer, S.; Fraschke, M.; et al. Ultra-fast germanium photodiode with 3-dB bandwidth of 265 GHz. *Nat. Photonics* **2021**, *15*, 925–931. [[CrossRef](#)]
56. Wang, J.; Cheng, Z.; Chen, Z.; Wan, X.; Zhu, B.; Tsang, H.K.; Shu, C.; Xu, J. High-responsivity graphene-on-silicon slot waveguide photodetectors. *Nanoscale* **2016**, *8*, 13206–13211. [[CrossRef](#)]
57. Ding, Y.; Cheng, Z.; Zhu, X.; Yvind, K.; Dong, J.; Galili, M.; Hu, H.; Mortensen, N.A.; Xiao, S.; Oxenløwe, L.K. Ultra-compact integrated graphene plasmonic photodetector with bandwidth above 110 GHz. *Nanophotonics* **2020**, *9*, 317–325. [[CrossRef](#)]
58. Wang, Y.; Li, X.; Jiang, Z.; Tong, L.; Deng, W.; Gao, X.; Huang, X.; Zhou, H.; Yu, Y.; Ye, L.; et al. Ultrahigh-speed graphene-based optical coherent receiver. *Nat. Commun.* **2021**, *12*, 5076. [[CrossRef](#)]
59. Yan, S.; Zuo, Y.; Xiao, S.; Oxenløwe, L.K.; Ding, Y. High-performance Silicon/Graphene Photodetector Employing Double Slot Structure. In Proceedings of the Conference on Lasers and Electro-Optics, San Jose, CA, USA, 9–14 May 2021; p. STh5B.2.
60. Schall, D.; Neumaier, D.; Mohsin, M.; Chmielak, B.; Bolten, J.; Porschatis, C.; Prinzen, A.; Matheisen, C.; Kuebart, W.; Junginger, B.; et al. 50 Gbit/s Photodetectors Based on Wafer-Scale Graphene for Integrated Silicon Photonic Communication Systems. *ACS Photonics* **2014**, *1*, 781–784. [[CrossRef](#)]
61. Ma, Z.; Kikunaga, K.; Wang, H.; Sun, S.; Amin, R.; Maiti, R.; Tahersima, M.H.; Dalir, H.; Miscuglio, M.; Sorger, V.J. Compact Graphene Plasmonic Slot Photodetector on Silicon-on-Insulator with High Responsivity. *ACS Photonics* **2020**, *7*, 932–940. [[CrossRef](#)]
62. Ma, P.; Salamin, Y.; Baeuerle, B.; Josten, A.; Heni, W.; Emboras, A.; Leuthold, J. Plasmonically Enhanced Graphene Photodetector Featuring 100 Gbit/s Data Reception, High Responsivity, and Compact Size. *ACS Photonics* **2019**, *6*, 154–161. [[CrossRef](#)]

63. Guo, J.; Li, J.; Liu, C.; Yin, Y.; Wang, W.; Ni, Z.; Fu, Z.; Yu, H.; Xu, Y.; Shi, Y.; et al. High-performance silicon–graphene hybrid plasmonic waveguide photodetectors beyond 1.55  $\mu\text{m}$ . *Light Sci. Appl.* **2020**, *9*, 29. [[CrossRef](#)]
64. Shiue, R.-J.; Gao, Y.; Wang, Y.; Peng, C.; Robertson, A.D.; Efetov, D.K.; Assefa, S.; Koppens, F.H.L.; Hone, J.; Englund, D. High-Responsivity Graphene–Boron Nitride Photodetector and Autocorrelator in a Silicon Photonic Integrated Circuit. *Nano Lett.* **2015**, *15*, 7288–7293. [[CrossRef](#)]
65. Schuler, S.; Schall, D.; Neumaier, D.; Schwarz, B.; Watanabe, K.; Taniguchi, T.; Mueller, T. Graphene Photodetector Integrated on a Photonic Crystal Defect Waveguide. *ACS Photonics* **2018**, *5*, 4758–4763. [[CrossRef](#)]
66. Schuler, S.; Muench, J.E.; Ruocco, A.; Balci, O.; van Thourhout, D.; Sorianello, V.; Romagnoli, M.; Watanabe, K.; Taniguchi, T.; Goykhman, I.; et al. High-responsivity graphene photodetectors integrated on silicon microring resonators. *Nat. Commun.* **2021**, *12*, 3733. [[CrossRef](#)]
67. Mišeikis, V.; Marconi, S.; Giambra, M.A.; Montanaro, A.; Martini, L.; Fabbri, F.; Pezzini, S.; Piccinini, G.; Forti, S.; Terrés, B.; et al. Ultrafast, Zero-Bias, Graphene Photodetectors with Polymeric Gate Dielectric on Passive Photonic Waveguides. *ACS Nano* **2020**, *14*, 11190–11204. [[CrossRef](#)]
68. Mauthe, S.; Baumgartner, Y.; Sousa, M.; Ding, Q.; Rossell, M.D.; Schenk, A.; Czornomaz, L.; Moselund, K.E. High-speed III-V nanowire photodetector monolithically integrated on Si. *Nat. Commun.* **2020**, *11*, 4565. [[CrossRef](#)]
69. Xue, Y.; Han, Y.; Tong, Y.; Yan, Z.; Wang, Y.; Zhang, Z.; Tsang, H.K.; Lau, K.M. High-performance III-V photodetectors on a monolithic InP/SOI platform. *Optica* **2021**, *8*, 1204–1209. [[CrossRef](#)]
70. Runge, P.; Zhou, G.; Ganzer, F.; Mutschall, S.; Seeger, A. Waveguide integrated InP-based photodetector for 100Gbaud applications operating at wavelengths of 1310nm and 1550nm. In Proceedings of the 2015 European Conference on Optical Communication (ECOC), Valencia, Spain, 27 September–1 October 2015; pp. 1–3.
71. Salamin, Y.; Ma, P.; Baeuerle, B.; Emboras, A.; Fedoryshyn, Y.; Heni, W.; Cheng, B.; Josten, A.; Leuthold, J. 100 GHz Plasmonic Photodetector. *ACS Photonics* **2018**, *5*, 3291–3297. [[CrossRef](#)]
72. Giambra, M.A.; Mišeikis, V.; Pezzini, S.; Marconi, S.; Montanaro, A.; Fabbri, F.; Sorianello, V.; Ferrari, A.C.; Coletti, C.; Romagnoli, M. Wafer-Scale Integration of Graphene-Based Photonic Devices. *ACS Nano* **2021**, *15*, 3171–3187. [[CrossRef](#)]
73. Kim, Y.; Kim, T.; Lee, J.; Choi, Y.S.; Moon, J.; Park, S.Y.; Lee, T.H.; Park, H.K.; Lee, S.A.; Kwon, M.S.; et al. Tailored Graphene Micropatterns by Wafer-Scale Direct Transfer for Flexible Chemical Sensor Platform. *Adv. Mater.* **2021**, *33*, 2004827. [[CrossRef](#)]